# Chamber Contour Design and Compression Flow Calculations of Rotary Engine

### Huai-Lung Ma\*, Cheng-Hsiung Kuo, and Chien-Chang Chen

Department of Mechanical Engineering, National Chung-Hsing University 250, Kuo Kuang Rd., Taichung 402, Taiwan R.O.C.

### **ABSTRACT**

Design of the chamber contours of a rotary engine is presented and, based on this design, the flow structure in each working chamber were calculated in this paper by way of CFD software (Fluent). It is found that increasing K factor (or R/e ratio) give a rotary engine with large rotor radius and small eccentricity. This will lead to high compression ratio, but low the leading angle of the apex seal. Besides, the CFD simulation is performed in each working chamber with inlet air flow by natural suction and with the air flow exhausted at the ambient pressure. During compression period, the simulated flow structures show two recirculation regions in the compression chamber and impinge onto the wall of rotor. This was believed to provide favorable effect on mixing of the air/fuel mixture before combustion occurs. In addition, the pressure distribution in the compression chamber is nearly uniform. This show the consistency with the assumptions suitable for the zero order thermodynamic analysis.

Keywords: rotary engine, compressible flow, CFD

### 轉子引擎燃燒室外型設計及壓縮流場計算

馬淮龍1\* 郭正雄2 陳建章3

1,3 國立中興大學機械工程研究所博士候選人 2 國立中興大學機械工程系教授

### 摘要

本文主要是進行轉子引擎的燃燒室與轉子外型設計,並依據設計結果來進行汽缸內壓縮流場計算。藉由提高轉子半徑及減少偏心距,使得無因次外型參數 K=R/e 逐級增加,結果顯示燃燒室內壓縮比值亦隨之同向增加,但是菱封導角卻呈反向降低;此外模擬外界空氣以自然進氣方式流入燃燒室內,結果發現流體在壓縮後的膨脹過程產生了二個迴流,將有助於燃燒行程中油料與空氣的混合。再者壓縮過程中汽缸內整體壓力分佈相當均勻,與熱力模式假設一致。

**關鍵字:**轉子引擎,可壓縮流場,計算流體

文稿收件日期 98.03.26; 文稿修正後接受日期 98.12.09; \*通訊作者 Manuscript received March 26, 2009; revised December 09, 2009.; \*Corresponding author

### 1. I. INTRODUCTION

### 1.1 The Characters of a Rotary Engine

The rotary engine (RE) is also called the Wankel engine because it was invented by German engineer Dr. Felix Wankel in 1957.; and its structure is shown below in Fig. 1. In RE, a three-sided symmetric rotor is located in the oval-like, epitrochoid-shaped housing, which is divided into three indpendent chambers. With an orbital revolution around the eccentric shaft, the four strokes (intake, compression, ignition, and exhaust) of a typical Otto cycle are generated consecutively within each chamber.

Furthermore, in contrast to the reciprocating engine, the rotor of the rotary engine is able to reach higher operation speed by continuously and smoothly operating in one direction without the need for precise balance of the crankshaft. The four strokes of the reciprocating engine complete one cycle for every two rotations (720°) of the transmission shaft; however, in rotary engine, due to the 1:3 rotation ratio of the rotor to the transmission shaft, the transmission shaft makes three rotations for every rotation of the rotor  $\alpha$ =[0,1080°]. With this clever design, RE can attain high power output with small mount of exhaust. In other words, the output power of RE can be twice that of the reciprocating engine with the same weight; or to attain the same output power, the intake volume of the rotary engine can be half that of a reciprocating engine. In addition, at the same rotation speed, the RE can take longer time elapse (1.5 times) to complete one stroke than that of a reciprocating engine. (Fig. 2).

### 1.2 Document Review

The researches focused on the RE are summarized in the following. Yamamoto (1971) clarified the ways to improve the performance of the rotary engine, such as minimizing the friction loss, enhancing the air sealing, improving the intake/exhaust port configuration as well as the timing, maintain at lean oil condition and suitable compression ratio. He also pointed out the important elements affecting the combustion of engine, such as the flame propagations inside the combustion chamber, the position of the spark plug, the contour of the combustion chamber

and the pattern of intake, etc. Danieli's study (1976) revealed that only increasing the compression ratio can not guarantee the enhancement of the engine performance because both increasing the compression ratio and reducing the cross section area of the passageway will increase airflow speed. This may cause a significant decrease of the heat release from the engine system and decreases the utilization of the combustion energy. In addition, reducing the cross section area of the passageway decreases the amount of the intake airflow, and will lead to longer combustion time and large quenching area. Danieli (1976) also pointed that the concaved rotor surface can help the flame to propagate through the narrow combustion chamber and enhance the combustion efficiency.

Norman (1983) employed a zero-order combustion model to test the performance of SCRE. His result showed that the leakage of the apex seal is the major reason that affects the performance of engine. Both low thermal energy utilization and crevice volume have minor influence on the performance of the engine under low loading condition; however, the above factors will have significant effect under high loading. Ohzeki & Yamaguchi (1983) concluded some possible ways to enhance the performance of RE in the following. (1) optimizing the position of spark plug and the shape of combustion chamber; (2) increasing the combustibility; (3) decreasing the loss of combustion energy; (4) decreasing the friction loss. Nguyen (1987) used the theoretical analysis to study the effects on SCRE performance based on the fuel equivalent ratio, the ignition timing, combustion rate, the volume loss of air sealing, the turbo-charging and compression ratio, etc. In his thesis, he pointed out the importance of understanding the combustion process for performance optimizing engine's efficiency. Muroki & Yoriyoshi's (1987) experimentally study the traditional spark plug and the pulse ignition systems. The study showed that combustion of lean oil in pulse ignition systems is superior to the spark

ignition system. Lee & Schock's (1988) established by experiment some empirical formula for the forced convective heat transfer coefficients (h) and Nu suitable to SCRE. Schock et al. (1989) measured flow field within **SCRE** through laser Doppler velocimeter. By doing so, they revealed some key parameters, that influence the SCRE combustion process, for the enhacing the combustion efficiency and the power density of the rotary engine. The intake and exhaust systems, the contour of rotor, the fuel injection, and friction due to the shaft and air seal were also investigated in this study.

Weston (1992) pointed out in rotary engine, the circular-arc-flank is necessary for increasing the compression ratio and thermal efficiency. During the manufacturing process, the rotor was made as circular as possible. With this design, the combustion chambers become narrower and the surface-volume ratio becomes too high. This design not only decreases the flammability of fuel-air mixture, and also makes the flame propagation more difficult, leading to poor utilization of the combustion energy. In order to overcome this deficiency, the recessed flank is implemented to improve the narrow combustion chamber. When the rotor is in the top or bottom positions, the two flank spaces are connected. The concave portion on the rotor is called rotor pocket. In addition, multiple spark plugs are often applied to improve the combustion quality in the narrow combustion chamber of RE.

Recently, the CFD had become a good tool for studying the related physics problems of heat and fluid flows because the simulation results can be a proper guidance for future experiments. Shih (1987) studied numerically the fuel-air mixture in the intake and compression process with a two-dimensional rotary engine. The key parameters in his study include the engine's speed and velocity (direction and magnitude) of fuel injection. Abraham & Bracco (1989a) studied a three-dimensional numerical simulation to compute the pressure field within the rotary engine with double spark plug using the

natural gas as the fuel. Their results are compared with the experimental data. The three-dimensional numerical simulation of Abraham & Bracco (1989<sup>b</sup>) further confirms the parameters controlling the combustion rate in the SCRE. In fuel atomization, the main ejector and the angle of air flow is quite important when it comes to facilitating the combustible gas mixtures. Raju & Willis (1990 a, b) employed a three-dimensional simulation to investigate the SCRE and considered the wake flame of the oil atomizer. They pointed out some key parameters for enhancing the combustion efficiency, such as the position of exhaust valve, the profile of the rotor pocket, the injector and spark timings, the fuel equivalence ratio and so on. Iron and Mount (1992)considered a three-dimensional simulation to study the performance of the SCRE influenced by the profile of the rotor pocket, and the velocity of fuel ejection. In their paper, they suggested the effects due to timing, the ignition-ejection position and the fuel-air ratio. Padmarajan (2004) employed simulate on the Fluent 6.1 to characteristics inside the combustion chamber of a rotary engine without intake and exhaust device. In his study, the dynamic mesh technique can deal well with the flow field in combustion chamber of rotary engine while the angle of transmission shaft is changing.

### 1.3 Application and Future Development

Mazda is the remarkable researcher and developer of RE in modern days. The new generation "Renesis" of RE is considered to be a perfect classics. This engine not only has high performance, high power and good feedbacks, it also has low levels of structural vibration, low pollution as well as low fuel consumption. In fact, the rotary engine is not limited to the automobile market only.

The Skycar volantor developed by Moller International is capable of vertical take-off and landing (VTOL) much as a helicopter. There are eight RE in the prototype. UAV Engines Ltd (UEL) also employed the RE to power the unmanned aerial vehicle (UAV) because of the compact size. In University of California at

Berkeley a research had been carried out to develop a micro RE, powered by liquid hydrocarbons, that will last 7-14 times longer than the conventional lithium or alkaline batteries.

### 2. II. CONTOUR DESIGN

### 2.1 Epitrochoidal Contour

Though both the RE and reciprocating engines are equipped with four-stroke Otto cycle, the contour of combustion chamber and the power mechanism are quite different. The contour of the combustion chamber in a rotary engine is epitrochiod, its outlook is just like an unshelled peanut. The circular-like on the top and bottom halves are flattened in the middle. The eccentric distance (e) and radius of rotor (R) are the main design parameters of the contours. The symbol A represents the rotation angles ranging between 0° and 360° The following shows the trajectory equations:

$$x = e \times \cos(3A) + R \times \cos(A)$$
  

$$y = e \times \sin(3A) + R \times \sin(A)$$
(1)

### 2.2 Selection of Design Parameter K

Several values of the parameter K=R/e are selected (9.6, 8.5, 7.4, 6.3, 5.2 and 4.1) to compare the corresponding contours and are shown. In Fig. 3, As the K value decreases, the profile in the middle becomes more concaved. In general, the intake and the exhaust ports are located on the concaved sides. If tip point in the middle of the concaved profile is used to separate the intake and exhaust ports, the intake and exhaust will operate independently with no interference. For industry applications, the K value lies most commonly between 6 and 8.

### 2.3 Maximum Compression Ratio $\varepsilon$ max

The efficiency of rotary engine is determined by the maximum compression ratio  $\varepsilon_{\rm max}$ . AS shown in equation 2, the value of  $\varepsilon_{\rm max}$  is also determined by the parameter K. As the K value increases, the value of  $\varepsilon_{\rm max}$  increases accordingly (Fig. 4), and vice versa.

From another respect, as the K value increases, the shape of combustion chamber becoming longer and narrower accordingly. This may cause uneven fuel distribution and poor flame propagation, leading to poor combustion quality. Therefore, a suitable K value in-between is required to get a compromise. Relative to the adjustment the compression ratio in reciprocating engine, selecting of suitable K value in designing the RE is very convenient.

$$\varepsilon_{\text{max}} = \left(\frac{\pi}{3} + 2\sqrt{K^2 - 9} + \left(\frac{2K^2}{9} + 4\right)\varphi_{\text{max}} + \frac{3\sqrt{3}}{2}K\right) / \left(\frac{\pi}{3} + 2\sqrt{K^2 - 9} + \left(\frac{2K^2}{9} + 4\right)\varphi_{\text{max}} - \frac{3\sqrt{3}}{2}K\right)$$
 (2)

### 2.4 Contour of Rotor

The major function of the rotor is to generate enough torsion output extracted from the combustion energy and drive the eccentric shaft and consequently the main transmission shaft. There are several mature editions for rotor's contour equations, we discuss Steinthorsson's (1988) two commonly used rotor's contour equations and sketch its outlines for comparison (Fig. 5). The rotor's contour equation as shown in equation 3, the apexes of triangle rotor are fully fay with the inner surface of cylinder, which is very for research and analysis on academic theory. The other rotor's contour equation as shown in equation 4, there are reserved gaps in-between apexes of triangle rotor and the inner surface of cylinder, this clever design with space is just nicely fill in by apex seal; it is valuable for practical applications of engine operation. Its equations are shown as the below sequence:

$$x = R\cos(2V) + (3e^{2}/R)(\cos(8V) - \cos(4V))$$

$$+ e(\cos(5V) + \cos(V))\sqrt{(1 - 9e^{2}/R)(\sin^{2}(3V))}$$

$$y = R\sin(2V) + (3e^{2}/R)(\sin(8V) - \sin(4V))$$

$$+ 2E(\sin(5V) - \sin(V))\sqrt{(1 - 9e^{2}/R)(\sin^{2}(3V))}$$

$$(3)$$

$$x = R\cos(2V) - (3e^{2}/R)(\sin(6V)\sin(2V))$$

$$+ 2E\cos(3V)\cos(2V)\sqrt{(1 - 9e^{2}/R)(\sin^{2}(3V))}$$

$$y = R\sin(2V) - (3e^{2}/R)(\sin(6V)\cos(2V))$$

$$+2e\cos(3V)\cos(2V)\sqrt{(1-9e^{2}/R)(\sin^{2}(3V))}$$
(4)

The V is the changing rotation angel in three valid sections, to obtain the outline for contour of combustion chamber.

The rotation angels from 30° to 90° form the rotor's surface 1.

The rotation angels from 150° to 210° form the rotor's surface 2.

The rotation angels from 270° to 330° form the rotor's surface 3.

Apex seal is another key component in RE, its material must have the properties of friction resisting and lubrication; for the use in aviation, apex seal need to be replaced periodically, about 250 aviation hours. In recent years, the newly developed technology of powder metallurgy solves the troublesome problem. The concave cannelure on the apex of triangle rotor can easily embed apex seal. To ensure no gas leak during the motive cycles in combustion chamber, the convex part of apex seal and the surface of cylinder must be closely contacted. The connection line between the center of triangle rotor and its apex, and the perpendicular line of apex seal adjacent to the surface of cylinder, the angle of these two straight lines is called apex seal's leading angle  $\varphi$ , referring to Fig. 6. According to the cosine theorem, the leading angle's equation is shown as equation 5; the greater the value represents the greater side stress on the apex seal, the value of  $\varphi$  is usually less than 30° to avoid from cracking.

$$\varphi = \cos^{-1}((K + 3\cos\frac{2}{3}\alpha) / (K^2 + 9 + 6K\cos\frac{2}{3}\alpha)^{1/2}) \quad (5)$$

When RE performs the periodically motive cycle, the value of  $\varphi$  also has miner changes periodically; the two major factors that affect the leading angel are the angel of main shaft  $\alpha$  and the contour parameter K. Fig. 7 shows the relationship between the rotation angel of main shaft and leading angel with different values of K. When the rotation angel of main shaft  $\alpha=3/2\pi$ ,  $3\pi$ ,  $9/2\pi$ ,  $6\pi$ , the leading angel has minimum value  $\varphi=0$ ; when the rotation angel of main shaft

 $\alpha$ =(3/2)cos<sup>-1</sup>(-3/K), the leading angel has maximum value  $\varphi_{\text{max}}$ =sin<sup>-1</sup>(3/K), the result shows the value of K is corresponding to the values of  $\varphi_{\text{max}}$ , and the value of  $\varphi_{\text{max}}$  decreases accordingly when the value of K increases.

### 2.5 Design Procedures

The following are the design procedures of rotary engine: (1) Determine the suitable max. The compression ratio  $\varepsilon_{max}$  based on the type of fuel and the material of cylinder. (2) Find the corresponding value of K in non-dimensional shape according to the value of  $\varepsilon_{max}$ , and sketch the contour of combustion chamber and rotor with a bit adjustment. (3) Find the maximum leading angel  $\varphi_{\text{max}}$  based on the value of K, and making a judgment whether the side stress is proper for apex seal, based on current material technology. The whole design procedures must iterate a few times for modification and to make sure every parts are according to and meeting the requirements, we then can proceed to next phase of prototype making and performance test.

# III. FLOW STRUCTURE SIMULATION

### 3.1 Geometry

Rotary engine's geometry module is shown as below Fig. 8. In rotary cylinder engine, the volumes of the three divided chambers change while rotor eccentrically rotates; A, B and C are assigned to these three chambers respectively and an observation point is set in chamber A (located at (-0.12,0.19) and marked as  $\bigstar$ )

### 3.2 Governing Equations

In order to simplify the complicacy of numerical computations, this study uses the followings as basic assumptions: (1) flow field is a two-dimensional non-stable flow field. (2)The working fluid is a compressible ideal fluid. (3)Surface of rotor and the outer shell are both in the non-slip and adiabatic condition. (4)

Based on k- $\epsilon$  pattern to solve turbulent flow field. (5) Ideal gas. The two-dimensional right-angle coordinates (x, y) is also applied, and based on mass, momentum and energy of conservation law to present the following continuity equations, momentum equations and energy equations respectively:

### **Continuity equations:**

$$\frac{\partial \rho}{\partial t} + \frac{\partial}{\partial x_i} (\rho u_i) = 0 \tag{6}$$

### **Momentum equations:**

$$\frac{\partial}{\partial t} (\rho u_i) + \frac{\partial}{\partial x_j} (\rho u_i u_j) = -\frac{\partial p}{\partial x_i} 
+ \frac{\partial}{\partial x_j} \left[ \mu \left( \frac{\partial u_i}{\partial x_j} + \frac{\partial u_j}{\partial x_i} \right) - \frac{2}{3} \delta_{ij} \frac{\partial u_l}{\partial x_l} \right] + \frac{\partial}{\partial x_j} \left( -\rho \overline{u_i' u_j'} \right) 
\delta_{ij} = \begin{cases} 0 & \text{if } i \neq j \\ 1 & \text{if } i = j \end{cases}$$
(7)

### k- $\varepsilon$ equations:

$$\frac{\partial}{\partial t} (\rho k) + \frac{\partial}{\partial x_{i}} (\rho k u_{i})$$

$$= \frac{\partial}{\partial x_{j}} \left[ \left( \mu + \frac{\mu_{t}}{\sigma_{k}} \right) \frac{\partial k}{\partial x_{j}} \right] - \rho \overline{u'_{i} u'_{j}} \frac{\partial u_{j}}{\partial x_{i}} - \rho \varepsilon$$

$$\frac{\partial}{\partial t} (\rho \varepsilon) + \frac{\partial}{\partial x_{i}} (\rho \varepsilon u_{i})$$

$$= \frac{\partial}{\partial x_{j}} \left[ \left( \mu + \frac{\mu_{t}}{\sigma_{\varepsilon}} \right) \frac{\partial \varepsilon}{\partial x_{j}} \right] - C_{1\varepsilon} \frac{\varepsilon}{k} \left( \rho \overline{u_{i}' u_{j}'} \frac{\partial u_{j}}{\partial x_{i}} \right) - C_{2\varepsilon} \rho \frac{\varepsilon^{2}}{k} \right]$$
(8)

### **Ideal gas equations:**

$$p = \rho RT \tag{9}$$

### 3.3 Initial Value and Boundary Condition

The initial conditions are set as follow: the entry velocity is zero and initial gage pressure is 0 atm; the boundary conditions of both entrance and exit gage pressures are set to 0 atm. The fluid's turbulence intensity is set to 5%.

It was necessary to develop a model which handles almost all the complexity of a practical RE. Dynamic mesh option available in the FLUENT 6.3 was explored and user defined function (UDF) was used in setting up

the RE model with stationary housing and rotating rotor. Again dynamic mesh model is used the shape of the domain is changing with time due to motion in the domain boundaries.

## 3.4 Dynamic Mesh Model with Rotating Rotor and Stationary Housing

The setting up of dynamic mesh model with rotating rotor and stationary housing is divided into three parts: (1). To set up a model having eccentric rotation of rotor. (2). To set up a model having a rotating part being in perfect contact with the housing. (3). After successfully developing the above two model the same ideal implemented into the RE model and carryout flow simulation.

The rotor is made to rotate about its Centre of gravity (CG) at three times the velocity of the eccentric rotation during one complete cycle in RE. Using linear velocity equation, rotation of the rotor over its CG is specified. A rotor rotating with angular velocity  $\beta$  at a radius R from the rotation centre at position R(t) has Cartesian coordinates:

$$x = r \times \cos(\beta t)$$
  

$$y = r \times \sin(\beta t)$$
(10)

To find the velocity above equation is differentiated with respect to time:

$$\dot{x} = -\beta r \times \sin(\beta t)$$

$$\dot{y} = \beta r \times \cos(\beta t)$$
(11)

In this case angular velocity  $\beta$  is given three times the value of omega.

Using DEFINE\_CG\_MOTION macro, motion of a rotary engine's dynamic zone can be specified by providing with the linear (vel) and angular velocity (omega) at every time step. FLUENT uses these velocities to update the node positions on the dynamic zone.

```
#include "udf.h"
#define r -0.034 /*Eccentricity*/
float beta;
DEFINE_CG_MOTION(rotor, dt, vel, omega, time, dtime)
{
    NV_S(vel, =, 0.0);
    NV_S(omega, =, 0.0);
    omega[2] = 314.16;
```

```
beta = 942.48;

vel[0] = -beta*r*sin(beta*time);

vel[1] = beta*r*cos(beta*time);

vel[2]= 0; }
```

### 3.5 Study Method

This study chooses US Fluent 6.3 as analysis tool; the major reason is its function of dynamic mesh. When simulating rotary engine's inner flow field, due to the closely orbital revolution against the outer shell of engine, the combustion chamber's volume varies according to the rotation angle of the eccentric shaft; therefore, this technique is required for simulation and there are about 25,682 non-structural computation mesh points. From another perspective, due to the tremendous pressure change of inner flow field in the rotary engine, the simulation in a compressible flow manner is required; however, this flow field's flow speed is still considering as low-speed flow, this type of flow field has the derivative Numerical Stiffness problem of compressible flow with low Mach number and the Preconditioning Technique is applied to solve this problem.

### IV. RESULTS

The CFD simulation is performed in each working chamber with inlet air flow by natural suction and with the air flow exhausted at the ambient outlet pressure on flow field with engine speed of 3,000 rpm. In the four-stroke rotary engine, all three working chambers are in continuous action.

When t\*=0, the entrance fluids are jetted into chamber A, and after they hit the rotor, they will then divide into two parts; some fluids will flow against the surface of rotor towards the direction of entrance, and form a small recurrent flow in the area between entrance and the apex of rotor, as shown in Fig. 9(a). Most fluids flow along the surface of rotor to (X, Y) = (0, 0.2), because of the direction of flow changes to upwards in the surrounding areas, these two fluids will divide into two again due to the influence from the contour geometry shape of engine. Most fluids

will flow towards the direction of entrance, and form a big recurrence flow on the top of chamber A. Small portions of fluid flow along the inner surface of outer shell. In the meantime, the fluids in chamber C which is connected to the exit flow towards the direction of exit, it is belonging to the process of exhaust and there is no recurrence flow occurs in chamber C. The chamber B with the smallest volume, it is belonging to the process of compression in the cycle of power output, therefore, there are less fluid lines in this chamber.

Fig. 9(b) shows: when rotor continue to rotate to t\*=1/8, the apex of rotor connect with the bottom part of entrance, the fluid also flow along the surface of rotor towards chamber A. and the fluids will still divide into two recurrence flow, one bigger and the other smaller in the chamber A. The reason for the occurrence of big recurrence flow is same as Fig. 9(a), it is still located on the top of chamber A. The small recurrence flow is the small portion of fluids flow along inner surface of housing and with the increasing of area of chamber A, it is formed when these fluids change the flow direction after hitting the rotor. In the moment when  $t^*=0$ , the small recurrence flow nearby the entrance disappear also because of the changing of area in chamber A. In addition, when t\*=0, the smallest area chamber B' area increases with the rotation of rotor, its process changes from compression to expansion.

When the time increases to t\*=3/8, Fig. 9(c) shows the chamber A which originally connected to the entrance has become a enclosed room, and its area in the chamber gradually become smaller along with the increasing time; there are still two small recurrence flows in chamber A, the smaller one has the tendency to enlarge and the bigger one shrinks otherwise. At the same time, the entrance and exist are connected via chamber C, the entrance flow form a recurrence flow because of blocking by the rotor in the entrance passageway. The area of chamber B continuously to increase, the most fluids are influenced by the rotation of rotor and flow

towards the direction of rotation, only small portion of fluids form a small recurrence flow after hitting the surface of rotor.

When the rotor reach to t\*=4/8, which is half of the power output in a cycle. From Fig. 9(d) we can find that the areas of chamber A decrease with the increasing of time. There are still two recurrence flows in chamber A, but both of them are getting smaller as it is already enter the compression process. The areas of chamber A continuously to increase, its flow field is similar to Fig. 9(c), and chamber C is still keep the entrance and exit connected, however, because of the increasing area nearby the entrance passageway, therefore, the recurrence flow shown in the Fig. 9(c) is no longer exist.

When t\*=5/8, chamber A continue to compress and its area decreases even more, there are still two recurrence flows in chamber A, but the big recurrence flow is obviously shrink. The most fluids in chamber B are influenced by the rotation of rotor; the area in chamber C continuously to enlarge, a small recurrence flow occurs on the top part where the entrance passageway connected with outer shell of rotor, as shown in Fig. 9(e).

When t\*=7/8, because the continuously to decreases in chamber A and lead to non existence of recurrence flow. And most fluids in chamber B will flow towards the exit due to the connection with exit, which means it turns from compression to expansion to exhaust. In this moment, the chamber C is connected with entrance, the entrance fluids flow into the chamber and hit the surface of rotor and divide into two, and will form two recurrence flows due to the area increasing in this chamber and the limitation of geometric shape, as shown in Fig. 9(f).

At last, when t\*=1 means the engine has completed one power output cycle, (Chamber A changes from intake to compress, chamber B changes from compression to exhaust, and chamber C changes from exhaust to intake) which means the flow field in chamber A will repeat the changing process of chamber B's flow field during t\*=1/8~7/8 before the next power output cycle starts. Similarly, chamber

B and chamber C will repeat chamber C and chamber A's flow fields during  $t*=1/8\sim7/8$ , respectively.

During the previous discussion, we already understand the flow condition of fluids in combustion chamber of rotary engine within one complete power output cycle. The following we view from a different angle, we use the instantaneous isobaric line map (the unit is pa) to observe and compare. Fig. 10(a) shows the inner pressure in chamber B is the greatest in all three chambers (during the process of compression) and the pressure is greater in the Y > 0 area than in the Y < 0 area. it is because the Y=0 area is the middle part of the geometric shape, and the naturally formed Nozzle flow passage will speed up the flow of fluids. The second greatest is chamber C (during the process of exhaust), and chamber A is the smallest (during the process of intake). The chamber A has three low-pressure areas. the lowest one is located at the position corresponding to the position of the big recurrence flow in Fig. 9(a); the other two low-pressure areas are corresponding to the small recurrence flow area and the area where the fluids flow along inner surface of outer shell, respectively.

When the rotor turns to t\*=1/8, chamber B is entering the process of expansion and exhaust from compression, the inner pressure in chamber B therefore is similar to t\*=0. The local pressure is higher nearby the chamber A, and the opposite apart from chamber A; however, the pressure in this chamber is still the greatest in all three chambers. The pressure in chamber A maintains the lowest in all three chambers and has two low-pressure areas; its location is same as where chamber A's location of big and small recurrence flows in Fig. 9(b). The inner pressure in chamber C is greater than the normal atmospheric pressure, as 10(b). During the time shown in Fig.  $t*=3/8\sim4/8$ , from Fig. 10(c), 10(d), demonstrates chamber A still has the lowest pressure among the three, it still have two low-pressure areas in chamber A and their locations are same as the locations of big and small recurrence flows in 9(c) and 9(d) respectively. The pressure in chamber B is still the highest among the three, however, the pressure decreases along with the increasing area of chamber; and chamber C continue to exhaust and start to intake, therefore, the inner pressure in chamber C will gradually decrease to the normal atmospheric pressure.

When rotor turns to t\*=3/8, chamber becomes an enclosed room, which means chamber A is changing from intake process to compression process. From Fig. 10(e), we know when t\*=5/8, chamber A's inner pressure has become greater than chamber B due to the continuously decrease of area in chamber A, however, the location of lower-pressure area in chamber A is still corresponding to the location of recurrence flow area in Fig. 10(d). The inner pressure continuously to decrease along with the increasing area in chamber B, and the inner pressure in chamber C is continuously to intake and exhaust, its pressure therefore is down to the standard atmosphere pressure. When  $t^*=7/8$ , chamber B is connected with the exit and starts to exhaust, the inner pressure in chamber B continuously to decrease and is still the second highest among the three chambers. Due to the continuously decrease of area, the chamber A's inner pressure continuously to increase and is still the highest among the three chambers, however, the inner lower-pressure areas are corresponding to the location of recurrence flow in chamber A. There is a low-pressure area in chamber C, its location is same as the location of small recurrence flow in chamber C as shown in Fig. 10(f).

From Fig. 11, we can understand pressure and temperature change on chamber A's observation point during one complete power cycle. Basically, the pressure in chamber A increases along with the increasing t\*, and its temperature also rises; the lower pressure will cause the temperature to drop, which means the pressure and temperature are direct proportional in engine's three chambers. In addition, at the moment in-between the temperature and pressure reach their maximum values and t\*=1, there is temperature and pressure values during this moment as the rotor passes through this observation point.

### V. CONCLUCTIONS

This paper is focus on the contour design of rotary engine's combustion chamber and design of rotor, also based on the result of design and the analysis on cold flow field with the numerical computation software Fluent. We simulate the natural air intake in the combustion chamber with the rotary engine's rotation speed of 3000 rpm, sum up the following conclusions:

- (1)The value of K affects the design of combustion chamber and contour design of rotor. Each value of K is corresponding to one  $\varepsilon_{\max}$  accordingly, and is also corresponding to one  $\varphi_{\max}$  accordingly. Sometimes we can use  $\varepsilon_{\max}$  or  $\varphi_{\max}$  to replace the value of K.
- (2) The value of K increases consecutively, the value of  $\varepsilon_{\max}$  increases accordingly, but the value of  $\varphi_{\max}$  decreases accordingly, and vice versa.
- (3)Successfully completed the simulation of compressible flow field in rotary engine's combustion chamber; especially applied the technique of Dynamic Mesh and set up the computational procedures.
- (4)From the result, we discovered that the intake air formed two recurrence flows due to the impact with the surface of rotor, which helped the mixture of fuel and air during the combustion process.

### NOMENCLATURE

Angle of rotation for housing

	8 8
V	Angle of rotation for rotor
R	Radius of rotor
e	Distance of eccentricity
α	Main shaft's rotation angle
β	Angular Velocity
$\varphi$	Apex seal's leading angle
3	Compression ratio
CG	Centre of gravity
RE	Rotary engine
UDF	User defined function
dt	Pointer to the dynamic zone data

Α

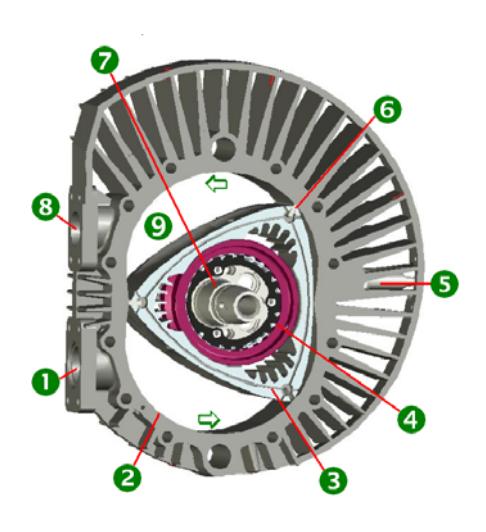
structure

dtime Time step supplied by FLUENT omega Angular velocity used in FLUENT vel Linear velocity used in FLUENT

### REFERENCES

- [1] Abraham, J., and Bracco, F. V., 1989<sup>a</sup>, "Fuel-Air Mixing and Distribution in a Direct-Injection Stratified-Charge Rotary Engine," SAE International Congress and Exposition, Detroit, Mich., SAE Paper No. 890329.
- [2] Abraham, J., and Bracco, F. V., 1989<sup>b</sup>, "Comparisons of Computed and Measured Pressure in a Premixed-Charge Natural-Gas-Fueled Rotary Engine," SAE International Congress and Exposition, Detroit, Mich., SAE Paper No. 890671.
- [3]Bartrand, T. A., and Willis, E. A., 1990, "Performance of a Supercharged Direct-Injection Stratified-Charge Rotary Combustion Engine," NASA Technical Memorandum 103105
- [4]Bartrand, T. A., and Willis, E. A., 1992, "Rotary Engine Performance Limits Predicted by a Zero-Dimensional Model," NASA Contractor Report 189129.
- [5] Çengel, Y. A., and Boles, M. A., Thermodynamics: An Engineering Approach, 3<sup>rd</sup> Edition, McGraw-Hill, Inc., New York.
- [6]Hoffman, T., Mack, J., and Mount, R., 1994, "Two Rotor Stratified Charge Rotary Engine (SCRE) Engine System Technology Evaluation," NASA Contractor Report CR-195395.
- [7] Irion, C. E., and Mount, R. E., 1992, "Stratified Charge Rotary Engine Critical Technology Enablement Volume I," NASA Contractor Report 189106.
- [8] Mount, R., 20003, "Advanced Propulsion Systems Study for General Aviation Aircraft", NASA/CR-2003-212334.
- [9] Nguyen, H. L., 1987, "Performance and Combustion Characteristics of Direct-Injection Stratified-Charge Rotary Engines," NASA Technical Memorandum 100134.
- [10] Norbve, J. P., 1973, "The Wankel engine," Chiton Book Company, Second Printing.
- [11]Raju, M. S., and Willis, E. A., 1990<sup>a</sup>, "Analysis of Rotary Engine Combustion Processes Based on Unsteady, Three-Dimensional Computations," NASA Technical Memorandum 102469.

- [12]Raju, M. S., and Willis, E. A., 1990<sup>b</sup>, "Computational Experience With a Three-Dimensional Rotary Engine Combustion MOdel," NASA Technical Memorandum 103104.
- [13]Schock, H., Hamady, F., and Somerton, C., "Stratified Charge Rotary Engine Combustion Studies," NASA-CR-197985.
- [14]Shih, T. I. P., 1987, "Numerical Simulation of the Flowfield in a Motored Two-Dimensional Wankel Engine," Journal of Propulsion and Power, Vol. 3, No. 3, pp. 269-276.
- [15]Steinthorsson, E., Shih, T.I-P, Schock, H.j., and Stegman, J., Calculations of the Unsteady, Three-Dimensional Flow Field Inside a Motored Wankel Engine, SAE International Congress and Exposition, Detroit, Mich., SAE Paper No. 880625, 1988.
- [16]Willis, E. A., and McFadden, J. J., "NASA's Rotary Engine Technology Enablement Program- 1983 Through 1991," NASA Technical Memorandum 105562.
- [17]Weston, K. C., 1992, Energy Conversion, 1<sup>st</sup> Edition, Brooks/Cole Publishing Co., New York.



- Intake Port
- .Housing
- ❸.Rotor
- 4.Internal Gear
- **⑤**.Spark Plugs
- 6.Apex Seal
- 2. Eccentric Shaft
- 3.Exhaust Port
- **9**.Combustion Chambers

Fig. 1. Wankel engine's structure.

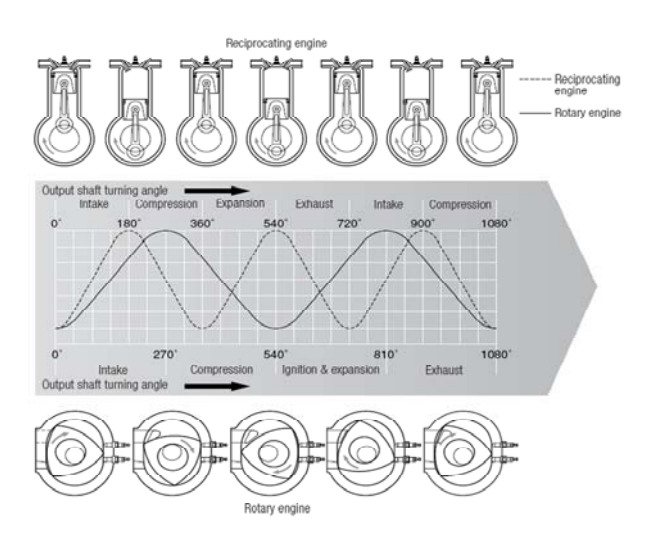


Fig. 2. Comparison of volume change for each stroke in the combustion chamber of rotary engine and reciprocating engine (Mazda, 2007).

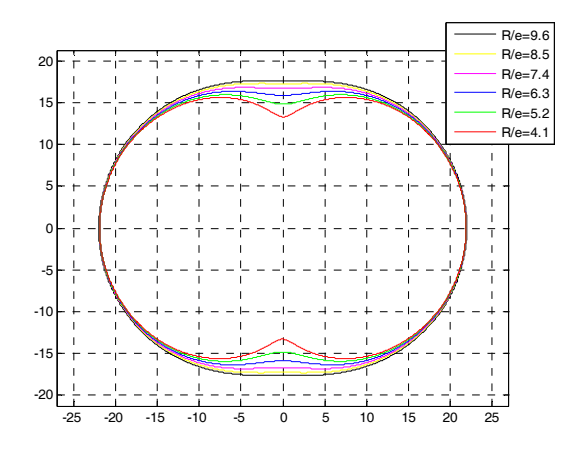
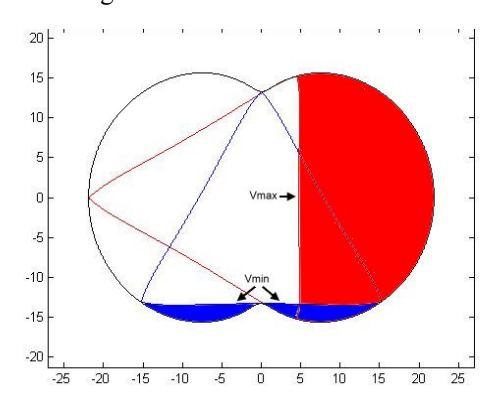
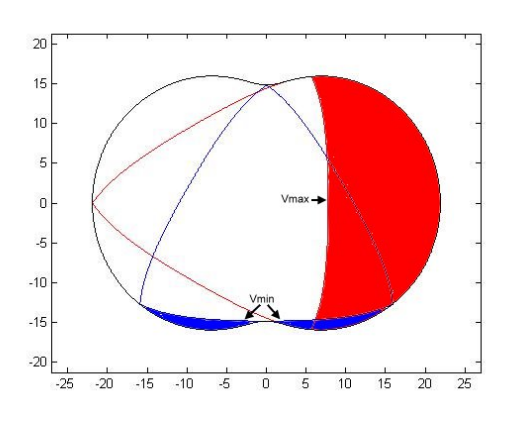


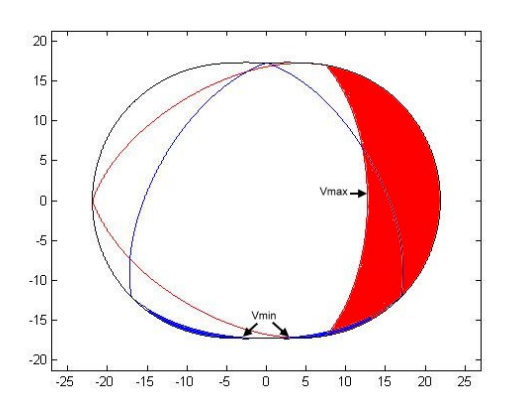
Fig. 3.The contour outlines with different values of contour parameter for the design of rotary engine's combustion chamber.



K = 4.1 ;  $\varepsilon_{\text{max}} = 10.23$  ;  $\phi = 47^{\circ}$ 



K=6.3 ; ε<sub>max</sub>=16.81 ; φ=28°



K=8.5 ;  $\epsilon_{max}\!=\!23.04$  ;  $\phi\!=\!21^{\circ}$ 

Fig. 4. The comparison diagrams of compression ratio and maximum leading angel of apex seal with different contour parameters in rotary engine.

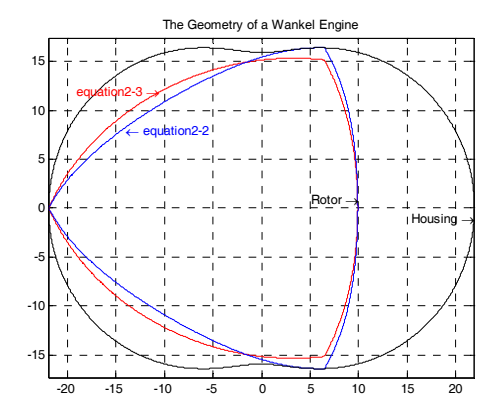


Fig. 5. The comparison diagram of two commonly used contour equations of rotor.

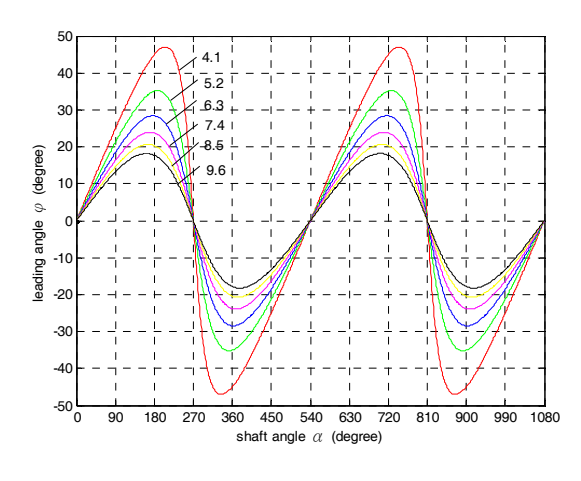


Fig. 6. The relationship between the rotation angel of main shaft and leading angel with different values of *K* in rotary engine.

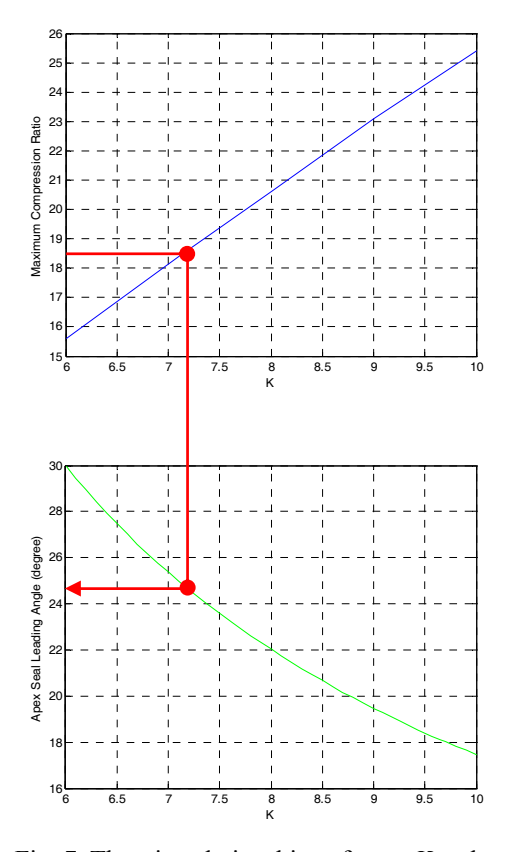


Fig. 7. The trio-relationships of  $\varepsilon_{\max}$ , K and  $\varphi_{\max}$  for rotary engine.

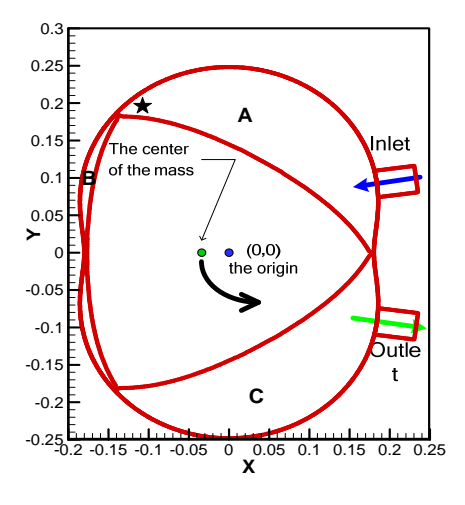


Fig. 8. RE's geometry module.

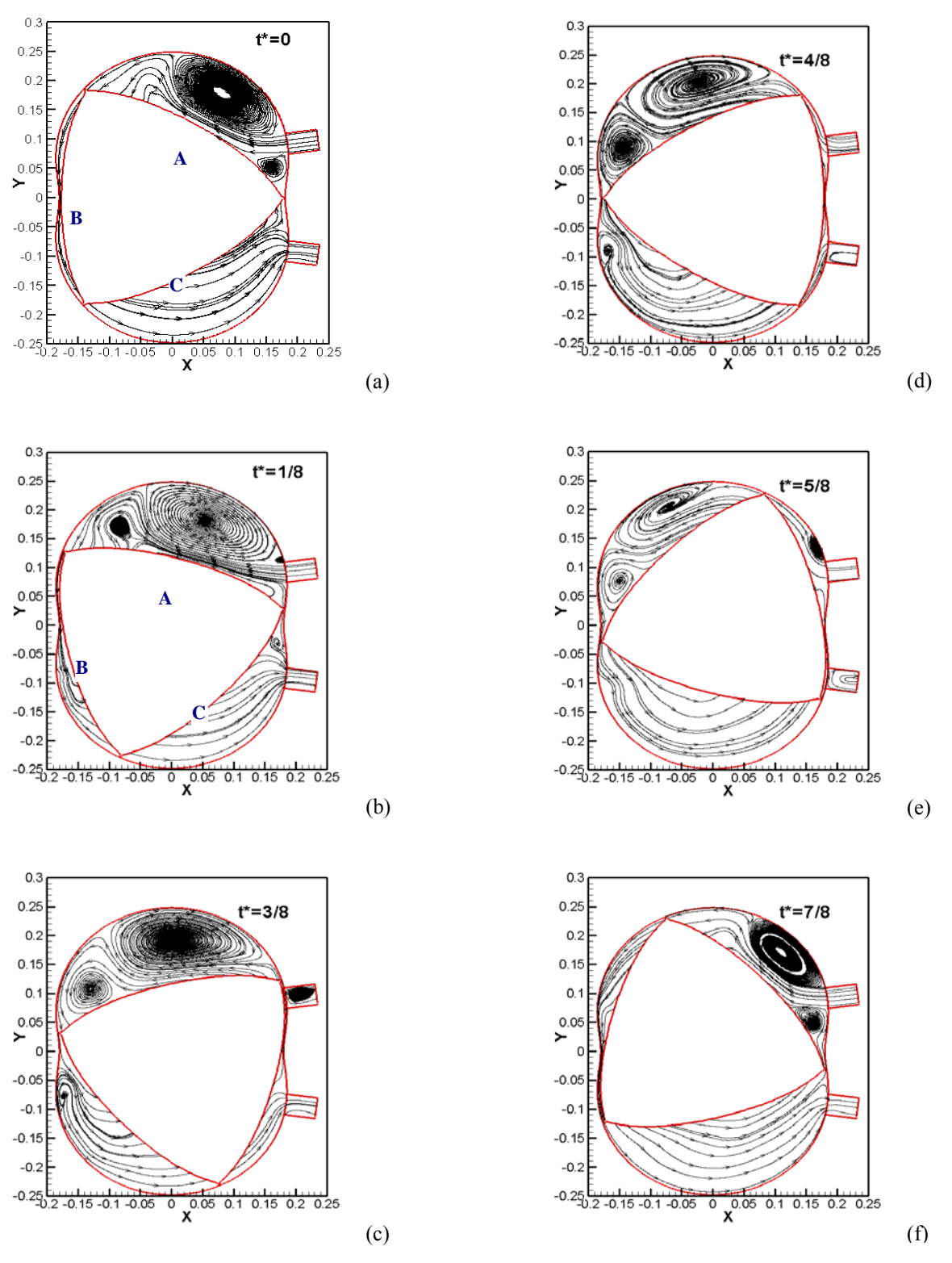


Fig. 9. The instantaneous flow lines with engine's rotation speed of 3000 rpm.

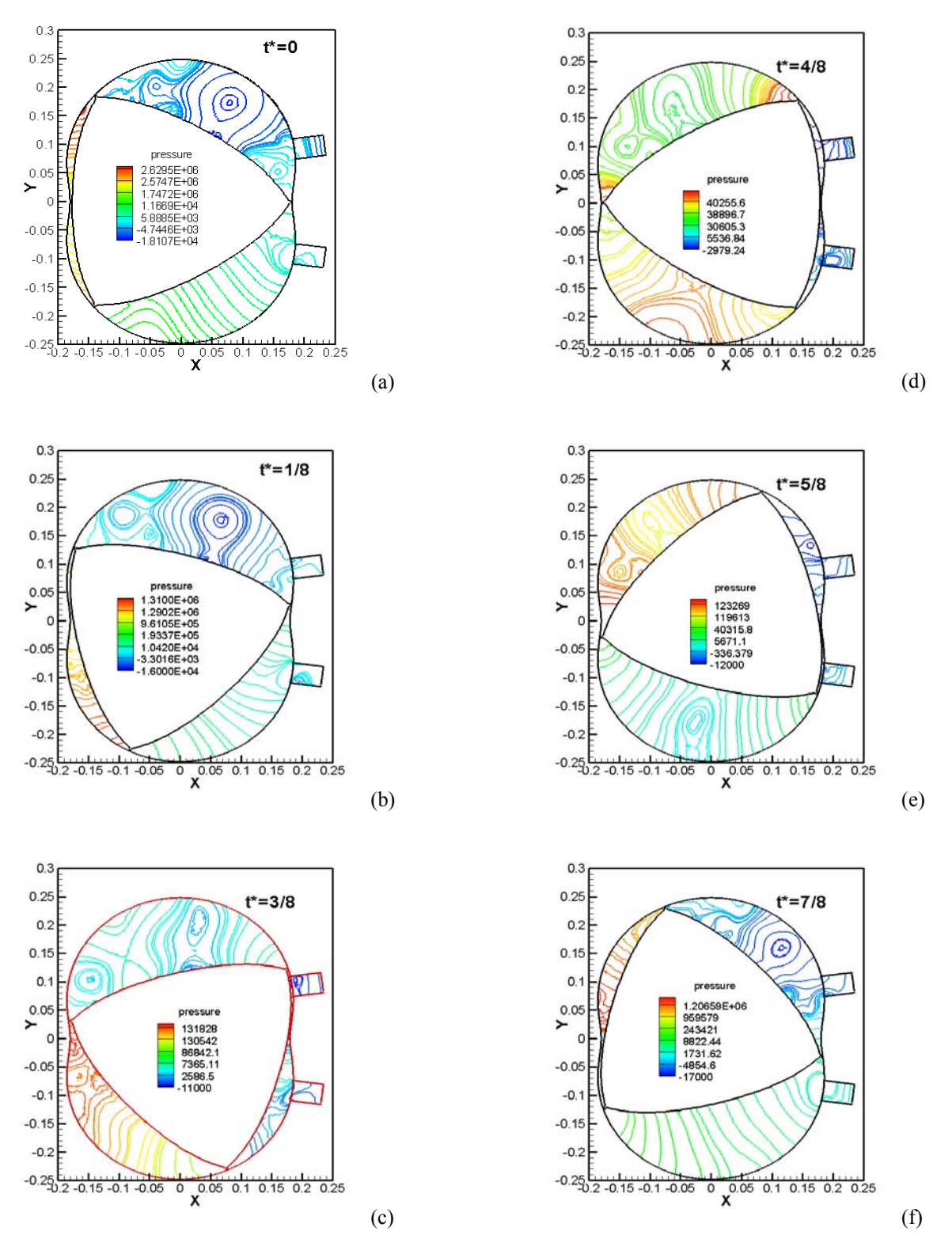


Fig. 10. The instantaneous pressure change with engine's rotation speed of 3000 rpm.

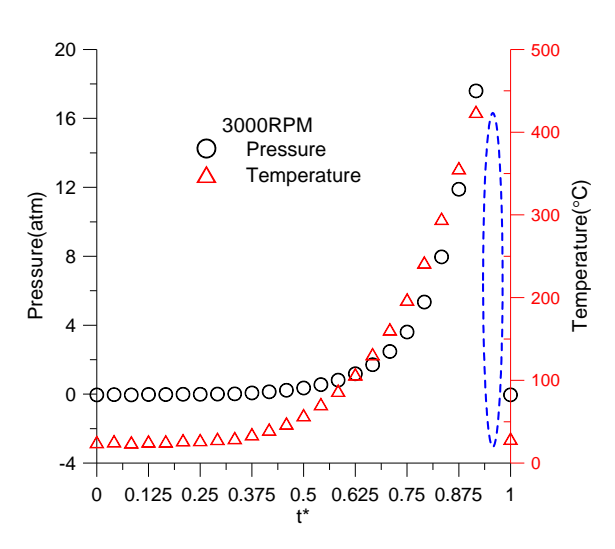


Fig. 11. Pressure and temperature change on engine's internal observation point (-0.12, 0.19) with engine's rotation speed of 3000 rpm.

Huai-Lung Ma, etc. Chamber Contour Design and Compression Flow Calculations of Rotary Engine